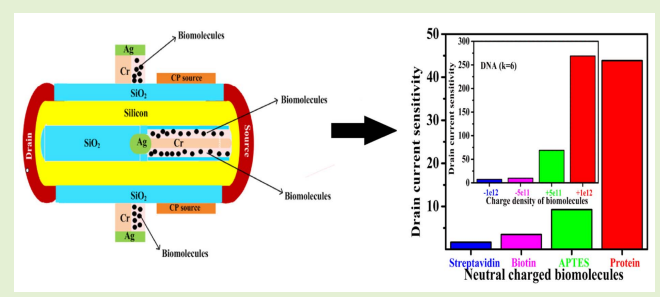


Design and Performance Assessment of Dielectrically Modulated Nanotube TFET Biosensor

Anju Gedam^{ID}, Graduate Student Member, IEEE, Bibhudendra Acharya^{ID}, and Guru Prasad Mishra^{ID}, Member, IEEE

Abstract—The manuscript proposes a novel charge plasma-based junctionless silicon dual cavity nanotube field-effect transistor (DC-NT-TFET) based biosensor for the detection of neutral and charged biomolecules. For improved sensing ability, the nanogap cavity is introduced in the inner as well as the outer portion of the NT-TFET. Also, the vertical orientation of the device enhances the even distribution of the biomolecules within the cavity area. The inner cavity provides more space for immobilization of the biomolecules and utilizes the advantages of material solubility. In this manuscript sensitivity of the proposed biosensor is investigated for four neutral biomolecules of dielectric constant, streptavidin ($k = .1$), biotin ($k = 2.63$), 3-aminopropyl-triethoxysilane (APTES) ($k = 3.57$), and protein ($k = 8$). Also, charged biomolecule, deoxyribonucleic acid (DNA) with a specific dielectric constant of $k = 6$ is examined for different positive as well as negative charge density. The sensing capability of the device is analyzed in terms of various DC and RF performance parameters. Also, outer cavity length optimization and on various biomolecules are analyzed in the manuscript.



Index Terms—Biosensor, DC/RF parameters, nanogap cavity, sensitivity.

I. INTRODUCTION

THE demand for devices that are user-friendly and have a fast response time to diagnose different diseases among the human population has been increased in the area of medical health care. The ability to measure health status, beginning of the disease, and sequence is the main aim to be achieved by medical health care type of equipment. The early syndrome finding is important for the patient's survival and successful prediction of the diseases so that high sensitivity and feasible structure are essential for the biosensors. The literature [1]–[6] includes the behavior of ion-sensitive field-effect transistor (ISFET), dielectric modulated field-effect transistor (DMFET), and field-effect transistor (FET) based label-free biosensors. An ISFET is used to sense the charged biomolecules, but it is unable to detect neutral biomolecules [7]. To overcome the drawback of an ISFET, DMFET was introduced, which can detect neutral as well as charged biomolecules effectively [8]. Apart from this, FET (bulk MOSFET) based

biosensors reported in [9]–[12] are used to enhance the sensing performance as compared to ISFET and DMFET biosensors. But scaling of the MOSFET-based biosensor devices into the nano-scale regime introduced some major limitations such as short channel effects (SCEs), kT/q limits, high static power consumption due to higher leakage, low I_{ON}/I_{OFF} ratio, low sensitivity, etc [3]–[5]. In this concern, the tunnel field-effect transistor (TFET) based biosensor has been widely investigated especially in dielectric modulated phenomenon [13]–[16]. Also, it overcomes the limitations of the MOSFET-based biosensor in terms of better sensing capability, smaller response time, energy-efficient, and lower leakage current. In this, biomolecules are detected by differences in the DC characteristics of the device because the biomolecules are present in the cavity region of the biosensor with different dielectric constants (k). In addition, the three-dimensional devices like nanowire TFET [17] and nanotube TFET based biosensors [18] enhance the sensing performance in various terms. Also, the three-dimensional devices provide more gate controllability, area-efficient, and improved electrical performance as compared to planar devices [19]–[23]. Moreover, the charge plasma based TFET provides uniform doping and a lower thermal budget with easy fabrication steps as the doping is not required to create individual source/drain regions [24].

In this manuscript, we proposed a dual cavity junctionless nanotube TFET (DC-JL-NT-TFET) biosensor, which is based

Manuscript received March 26, 2021; revised April 5, 2021 and April 26, 2021; accepted April 27, 2021. Date of publication May 17, 2021; date of current version July 30, 2021. The associate editor coordinating the review of this article and approving it for publication was Prof. Janice Limson. (Corresponding author: Guru Prasad Mishra.)

The authors are with the Department of Electronics and Communication Engineering, National Institute of Technology Raipur, Raipur 492010, India (e-mail: anju.phd2018/etc@nitrr.ac.in; bacharya/etc@nitrr.ac.in; gpcsmishra/etc@nitrr.ac.in).

Digital Object Identifier 10.1109/JSEN.2021.3080922

on core-shell architecture. The source and channel regions are formed with an appropriate metal workfunction by charge plasma technique. A core-shell or nanotube structure is a novel device it has dual-gate (inner and outer) all around, which increases the electrostatic controllability of the gate over the channel region. It also carries the properties of scaling down the structures into the nano-scale regime.

The advantage of including the core gate inside the shell is to minimize the quantum effect and stray charges. Therefore, we have investigated the DC-NT-TFET for sensing applications. In the proposed device two cavities are introduced in inner and outer cylindrical parts to improve the sensing capability of the device. The inner cavity is introduced in the inner source section, and the outer cavity is created in a half portion of the channel up to the gate towards the source region. The dual cavity of the device effectively senses the presence of biomolecules within it. The presence of biomolecules in cavity area increases the capacitive coupling, which results in an improvement of the electrical characteristics of the biosensor.

In this work, both the cavities are filled with neutral biomolecules of different dielectric constant such as streptavidin ($k = 2.1$, used for detection of lipid, nucleic acid, and protein), biotin ($k = 2.63$, is a vitamin B which is found in foodstuff, helps to manage blood sugar, and also the growth of nails and hairs), 3-aminopropyl-triethoxysilane (APTES) ($k = 3.57$, used for the treatment of acidic oil-in-water emulsions), and protein ($k = 8$, used for repair tissue and make hormones) [14], [25]–[27]. Moreover, the charged biomolecules are also detected through biosensors, where the deoxyribonucleic acid (DNA) range of dielectric constant is approximately ($K = 6$) dedicated to DNA [3]. Here we analyzed DNA at constant dielectric $k = 6$ for different values of charge density (positive and negative). The sensitivity of the device for the presence of different biomolecules is calculated when both the cavity is filled with air ($k = 1$). Unlike previously reported dielectrically modulated biosensors, the sensitivity of the biosensor is analyzed in terms of various DC as well as RF performance parameters. The detailed analysis of the proposed biosensor has been discussed for neutral and charged biomolecules in the manuscript.

II. MODEL VALIDATION

The device model is calibrated with previously published conventional charge plasma-based NT-TFET [28], after bringing all the dimensions and biasing conditions of the device. The I_{DS} - V_{GS} of the charge plasma-based NT-TFET biosensor is approximately following the reported curve.

III. DEVICE STRUCTURE, MODEL DETAILS AND FABRICATION PROCESS

A. Device Structure Specification

The device is designed by N-type junctionless silicon via charged plasma technology. The biosensor is a nanotube style and is structured vertically in a wafer. In the charge plasma concept, the P+ source region can be formed using a suitable metal workfunction. The source metal should be followed, $\Phi_S > \chi_{Si} + (E_g/2)$, where Φ_S is the workfunction of source

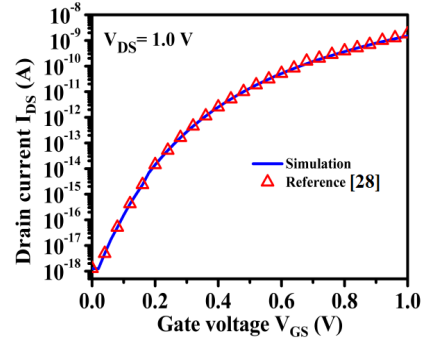


Fig. 1. 3D calibrated simulation result of [28].

metal, χ_{Si} is electron affinity of silicon ($\chi_{Si} = 4.17$ eV) and E_g is the energy bandgap of silicon. Also, it should follow the Debye length ($L_D = [(e_{Si} \cdot V_t)/(qN)]^{0.5}$), where Φ_{Si} , V_t , q , and N are the dielectric constant of silicon, threshold voltage, the charge of the electron, and intrinsic carrier concentration of the silicon respectively [29]. So, the thickness of the silicon body for the formation of charge through the metal electrode is less than Debye length. For the creation of the P+ source region, platinum metal with the workfunction of 5.93eV is used. In addition, both inner and outer gates are divided into two connecting gates named Gate 1 and Gate.

The Gate1 and Gate consist of chromium (Cr) and silver (Ag) with the workfunction of 4.37eV and 4.45eV, respectively. The lower workfunction of Ag is taken, which is used in the low-power devices, so that biosensor is turned on at a lower bias of applied voltage. The inner and outer cavities are formed by etching Cr metal; the thin layer deposition and uniform etching are possible by using Cr in the biosensor. Also, Cr and Ag together show outstanding chemical bonding and mechanical strength, which provides essential stability to the biosensor [3], [6], [30]–[32].

Moreover, in the proposed biosensor with the shifted inner gate, in the half portion of the channel region is taken near the source/channel interface. In the schematic structure of 2-D and 3-D of the biosensor, creating the cavity (inner and outer) is shown in Fig. 2(a) and (b) respectively. The 10nm diameter of silicon body and inner gate of Ag is considered for the DC-NT-TFET biosensor device. The outer cavity is projected from half of the channel area of 10nm towards the source region. Further, the inner cavity is created in the source region, which improves the even distribution of the biomolecules. Apart from the source, drain and the channel lengths are considered as 50, 50, and 22 nm, respectively. The outer gate and outer charge plasma electrode lengths are taken as 20 nm and 50nm, respectively. Difference between outer gate and charge plasma source is 2nm. The silicon body is covered with 1nm thick outer oxide (SiO_2) material.

B. Model Details

To evaluate the effectiveness of the proposed device for biosensing application, different neutral and charged biomolecules are filled into the cavity to analyze their behavior on different electrical parameters. The simulation has been

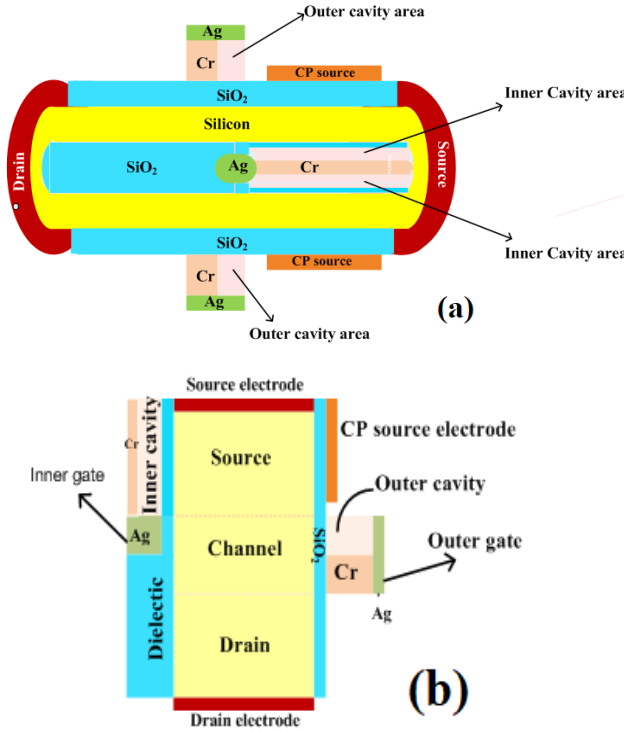


Fig. 2. (a) 3-D structure (b) One half vertical 2-D schematic structure of DC-NT-TFET biosensor.

done by the TCAD Silvaco simulator [33]. The proposed biosensor simulation has been performed considering various physical models. The **BBT.KANE** model has been introduced for consideration of the nonlocal band to band tunneling. Moreover, **CONMOB** and **FLDMOB** include concentration and field-dependent mobility, SRH, and AUGER models considered for recombination in the semiconductor. Apart from this, Fermi Dirac statistics with Boltzmann approximation is applicable in the modeling of band structures. The gummel newton maxtrap approximation is used for calculation of the physical model in a mathematical form.

C. Fabrication Process

At the experimental level, the fabrication process of a charge plasma P–N diode is already demonstrated in [34]–[35]. The traditional nanotube TFET fabrication process is also suggested in the literature [19]–[20], [36]. The proposed nanotube TFET biosensor is a combination of charge plasma nanotube concepts. This structure further extends in terms of cavities for biosensors. The fabrication process flow of the DC-NT-TFET biosensor shows in Fig. 3(step [1]–step [28]). The design of this biosensor is proposed to grow vertically to simplify the fabrication process of the device using a sacrificial layer. The fabrication of the DC-NT-TFET biosensor begins with an equally doped substrate of the N⁺ type with the same doping concentration ($1 \times 10^{18} \text{ cm}^{-3}$) in the silicon wafer (step [1]). The outer cylindrical part can be obtained by dielectric and sacrificial oxide using electron beam lithography (EBL) and etching (step [2]). The outer gate oxide (SiO₂) and gate metal (Cr) are proposed to be deposited in (step [3]) and

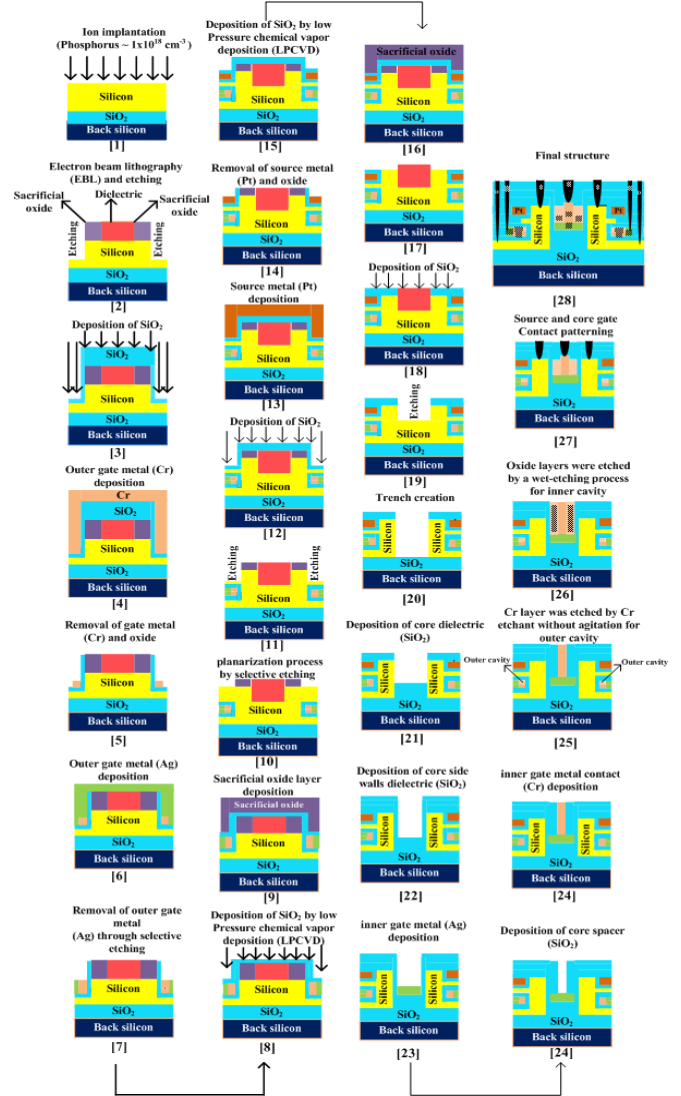


Fig. 3. Fabrication process of DC-NT-TFET biosensor.

(step [4]), respectively. Later the outer gate oxide and gate metal (Cr) must be partially removed (step [5]). The channel cavity region can be constructed by using chromium (Cr).

The deposition of outer gate metal (Ag) in (step [6]), and removal of Ag through selective etching can be performed in (step [7]). For gate oxides and spacer oxides, SiO₂ should be used to simplify the process of manufacturing nanotubes, as base silicon. For avoiding the direct contact between outer gate metal (Ag) and source metal (Pt), SiO₂ can be deposited by low-pressure chemical layer deposition (LPCVD) (step [8]). Sacrificial oxide layer deposition (step [9]) and the planarization process are to be done by using selective etching (step [10]). Space for the outer source metal electrode can be created by using selective etching (step [11]). In addition, the deposition of outer oxide (step [12]) and source metal (Pt) must follow to create the P⁺ source region (step [13]). For the creation of the source region, platinum (Pt) metal may be used in the fabrication process. This allows for transformational function by inducing halogen adsorption onto Pt (111) as a

function of coverage without affecting the reliability of the dielectric [37].

Later, the source metal (Pt) and oxide are partially to be removed (step [14]), and SiO_2 can be deposited by LPCVD (step [15]). Subsequently, the sacrificial oxide layer can be formed (step [16]) and removed (step [17]). To create a trench for the inner part of the device, SiO_2 is to be deposited (step [18]) and etching will be performed in the proposed device (step [19], [20]). The spacer must be formed in the inner section (step [21]), and again a thin layer of oxide is deposited in the inner portion of the device (step [22]) to avoid direct contact between the inner gate metal (Ag and Cr) and silicon. The deposition of core gate metal (Ag) (step [22]) and core spacer (step [23]) can be performed for the proposed device. After that, inner gate metal contact must be deposited (step [24]). The deposition of core gate metal (Ag) (step [22]) and core spacer (step [23]) will be performed for the proposed device. After that, inner gate metal contact can be deposited (step [24]). Further, the outer Cr layer must be etched by Cr etchant (step [25]). Later, the inner oxide layer can be etched by the wet etching process, which creates an internal cavity (step [26]). Finally, gate contact for the inner section and drain, source, and gate for the outer portion can be provided for the proposed biosensor (step [27], [28]).

IV. RESULTS AND DISCUSSION

A. DC Characteristics and Sensitivity

To reflect the fundamental function and physics of the proposed biosensor, some physical characteristics are investigated. This section contains the electrostatic behavior of the proposed DC-NT-TFET biosensor with the variation of different dielectric constant for neutral biomolecules and various charge density (positive and negative) for charged biomolecule. Fig. 4 (a) shows the energy band diagram under ON-state for various neutral biomolecules with different dielectric constant present at the cavity of the biosensor. Here, it is seen that as the dielectric constant of the biomolecule increases, the capacitive nature of the device increases, results in the decrease of tunneling barrier of the source/channel junction. Smaller tunneling barrier found for the protein biomolecule, which has higher dielectric constant of $k = 8$. Accordingly, in Fig. 4(b) the electric field depicts a similar behavior. More reduction in the tunneling barrier, increases the electric field across the source/channel junction. The highest peak of the electric field is obtained for protein, which has the highest dielectric constant among all the neutral biomolecules.

Fig. 5 (a) and (b) shows the transfer characteristics of different neutral and charged biomolecules, respectively. In Fig. 5 (a), protein shows the higher drain current due to higher tunneling, which is responsible for lesser tunneling barrier width and electric field at the source/channel as already seen in Fig 5(a-b). It is examined that increment in the drain current with increment in the dielectric constant of neutral biomolecules as the capacitance is directly proportional to the dielectric constant. Similarly, Fig. 5(b) shows the transfer characteristics for DNA for different values of charge density. For DNA, enhancement in the drain current with increment in the positive charge biomolecule and degradation with

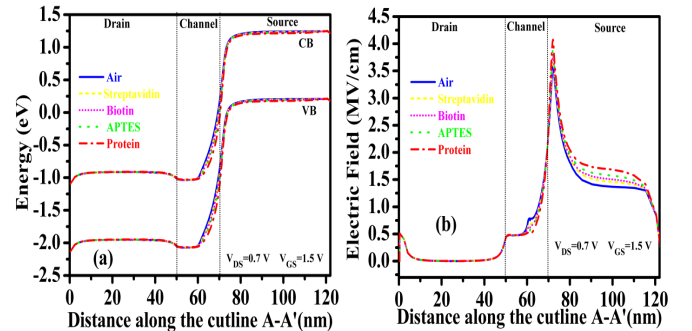


Fig. 4. (a) Energy band diagram (b) Electric field under ON-state for various neutral biomolecules.

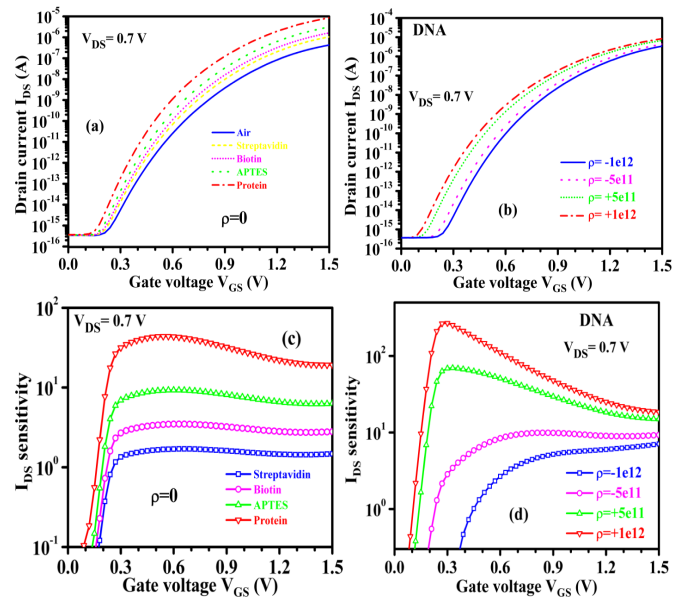


Fig. 5. Transfer characteristics (a) neutral charge biomolecules (b) charged biomolecules (DNA) and I_{DS} - V_{GS} Sensitivity plot of (c) neutral charge biomolecules (d) charged biomolecules (DNA).

increasing in negative charge biomolecules is observed. This is because positive charge biomolecules enhance the number of electrons and negative charge biomolecules present in the cavity, enhances the number of holes in the channel region. This increases/decreases tunneling of electrons through the barrier for positive/negative charged biomolecules respectively. The work presents the sensitivity of the biosensor in terms of some DC parameters like drain current (I_{DS}), subthreshold swing (SS), threshold voltage (V_{th}), and I_{ON}/I_{OFF} sensitivity.

Investigation of sensitivity in the biosensor is the parameter to identify the variation of target biomolecules for the air present in the cavity in the form of electrical parameters. Higher sensitivity defines the highest probability to detect the targeted biomolecules [38]. The drain current sensitivity is defined as [15], [38]:

$$S_{IDS} = \left| \frac{(SS_{IDS(Bio)} - SS_{IDS(Air)})}{SS_{IDS(Air)}} \right| \quad (1)$$

where, $SS_{IDS(Bio)}$ and $SS_{IDS(Air)}$ denotes the presence and absence of biomolecules in the cavity region. Fig. 5(c) and (d)

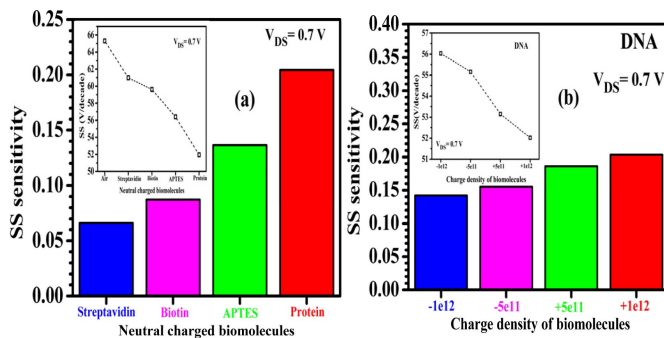


Fig. 6. (a) Subthreshold swing (SS) Sensitivity plot of (a) neutral charge biomolecules (b) charged biomolecules (DNA).

represents the drain current sensitivity to gate voltage for neutral and charged biomolecules for different dielectric constant and charge density (positive and negative) respectively.

In Fig. 5(c), as the dielectric constant of the biomolecule increases the drain current sensitivity increases. Streptavidin shows the lowest and protein shows the highest sensitivity as compared to all other biomolecules. The significant thing about the drain current sensitivity is that the highest peak is attained at the lower gate voltage V_{GS} .

SS sensitivity plays a vital role in the biosensor performance, which describes the speed of the detection of the biomolecules. SS sensitivity can be defined as:

$$SSS = \left| \frac{(SS_{(Bio)} - SS_{(Air)})}{SS_{(Air)}} \right| \quad (2)$$

where, $SS_{(Air)}$ and $SS_{(Bio)}$ signifies the SS when the biosensor cavity is occupied with biomolecules (neutral and charged) and air, respectively. Fig. 6(a-b) represents the SS sensitivity for neutral and charged biomolecules. Smaller value of SS gives the superior detection potential and enhanced electrical response of DC-NT-TFET biosensor. Here, it is seen that reduction of SS with increment in the dielectric constant of biomolecules from the air ($k = 1$) to protein ($k = 8$) in Fig. 6(a). Also, SS sensitivity increases from streptavidin ($k = 2.1$) to protein ($k = 8$). It signifies that, sensitivity increases with enhancement in dielectric constant of the biomolecule. Similarly, Fig. 6(b) shows the charge biomolecule (DNA) for different charge density, the SS of the device rises with rise of negative charge density and drops with higher positive charge density. Also, the change in the charge density from negative to positive causes enhancement in the SS sensitivity of the proposed biosensor.

The threshold voltage (V_{th}) calculation can be done by using the constant current method, where the voltage at drain current $1 \times 10^{-7}\text{ A}$ is considered as V_{th} [39], [40]. The V_{th} sensitivity parameter is defined as [15]:

$$\Delta V_{th} = |\Delta V_{th(Air)} - \Delta V_{th(Bio)}| \quad (3)$$

In this expression, $V_{th(Air)}$ and $V_{th(Bio)}$ represent the threshold voltage when the cavity is filled with air and biomolecules respectively. Also, ΔV_{th} is the shifting of threshold voltage during the detection of biomolecules for air. In Fig. 7(a) inset shows the relative V_{th} , where V_{th} decreases as the cavity

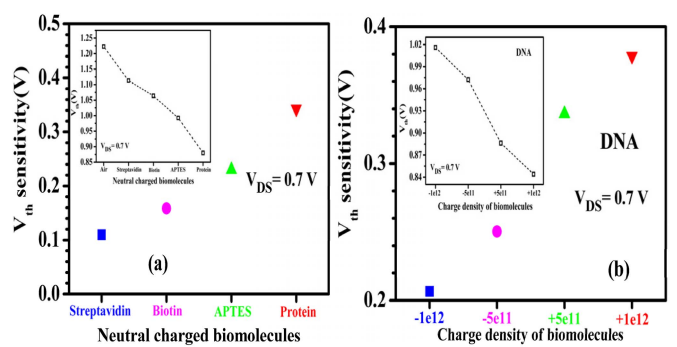


Fig. 7. (a) Threshold voltage (V_{th}) sensitivity plot of (a) neutral charge biomolecules (b) charged biomolecules (DNA).

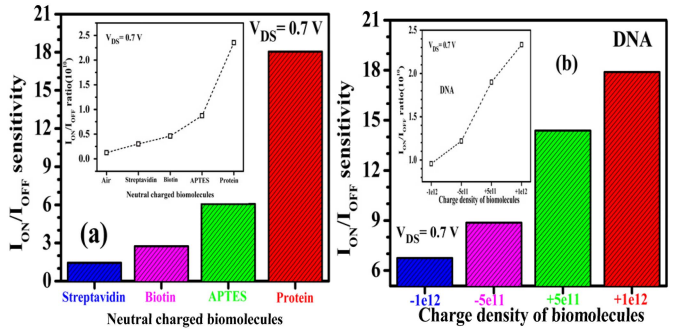


Fig. 8. I_{ON}/I_{OFF} ratio sensitivity plot of (a) neutral charge biomolecules (b) charged biomolecules (DNA).

is filled with a higher dielectric constant of biomolecules. So, the drain current reaches 1×10^{-7} sooner as compared to air. The V_{th} sensitivity is measured by using equation (3), where the protein ($k = 8$) shows the highest sensitivity among all neutral biomolecules. In the same manner, Fig. 7(b) inset shows a higher V_{th} value for more negative and lesser value of V_{th} for more positive charge density of DNA. Also, the V_{th} sensitivity is increasing from negative to positive charge density.

The I_{DS} sensitivity is calculated from equation (1) and similarly I_{ON}/I_{OFF} sensitivity is also determined. In Fig. 8(a), I_{ON}/I_{OFF} ratio increases with the rise of dielectric constant within the nanogap cavity, because the tunneling barrier at the source/channel interface reduces and this results in a higher electron tunneling rate from source to channel region.

So, the protein ($k = 8$) biomolecule in the nanogap cavity shows the highest I_{ON}/I_{OFF} ratio sensitivity among all neutral biomolecules. Fig. 8 (b) shows that for DNA biomolecules both I_{ON}/I_{OFF} ratio (in the inset) as well as I_{ON}/I_{OFF} sensitivity increases with increment in the charge density either it is positive or negative. The reason is immobilization of higher charge density within the cavity along with gate voltage leads to a better inversion under the cavity. The tunneling barrier reduces at source/channel interface due to formation of abrupt tunneling junction.

B. RF Characteristics and Sensitivity

This work is not only limited to the DC parameter sensitivity investigation, but the Radio frequency (RF) figures of

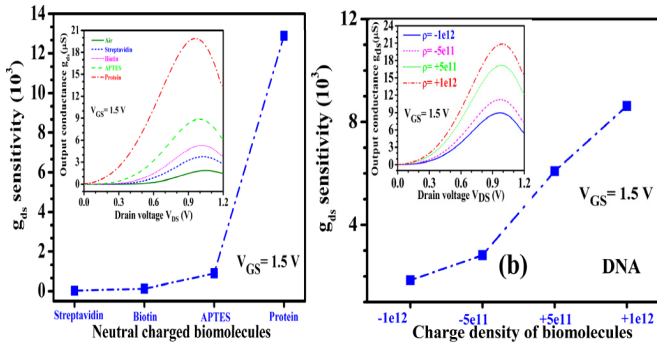


Fig. 9. Output conductance (g_{ds}) sensitivity plots of (a) neutral charge biomolecules (b) charged biomolecules (DNA).

merit (FOMs) sensitivity parameters have also been found. For the calculation of the RF sensitivity parameter, the air is considered as reference. Further, the RF sensitivity of the biosensor is calculated by the given formula throughout the manuscript for RF parameters.

$$\text{sensitivity} = \left| \frac{(Q_1 - Q_2)}{Q_1} \right| \quad (4)$$

where, Q_1 is the quantity when air ($K = 1$) is present in the nanogap cavity and Q_2 is the quantity when the different dielectric (neutral and charged) biomolecules are present in the nanogap cavity of the biosensor. The output conductance (g_{ds}) is an important parameter to determine the dependency of the I_{DS} on V_{DS} . Fig. 9(a) shows the g_{ds} (inset) with V_{DS} and g_{ds} sensitivity (outset) for different neutral biomolecule. From the observation g_{ds} increases with V_{DS} and with increment of dielectric constant of biomolecules from $k = 1$ to 8 (protein); at $V_{DS} = 0.9$ V, g_{ds} has the highest peak for protein. The figure also reveals the negligible variation in g_{ds} sensitivity up to APTES, but further a huge rise is observed for protein. In Fig. 9(b), impact of charge density of charged DNA molecules is investigated over g_{ds} and g_{ds} sensitivity. The g_{ds} and g_{ds} sensitivity both increases with charge density; inset reflects the variation of g_{ds} with V_{DS} also for different DNA charge densities, a peak in g_{ds} can be observed near 0.9 V of V_{DS} .

The transconductance (g_m), describes the ability of the device to convert the applied gate voltage into drain current. In addition to this, the cut-off frequency (f_T) is defined as the frequency at which current gain, turn into unity in the small-signal model of common source configuration; f_T can be expressed as:

$$f_T = \frac{g_m}{2\pi(C_{gs} + C_{gd})} \quad (5)$$

The g_m and f_T are analyzed in Fig. 10(a-d) for different neutral and charged biomolecule.

All the figures (insets) depict that enhancement of g_m and f_T value with an increment in the dielectric constant and charge density of biomolecules within the cavity. Fig. 10(a-b) shows that protein ($k = 8$) and positive charge density (+1e12) of DNA has highest peak sensitivity of g_m . Variation in the g_m with applied V_{GS} is detected. Therefore, a transconductance

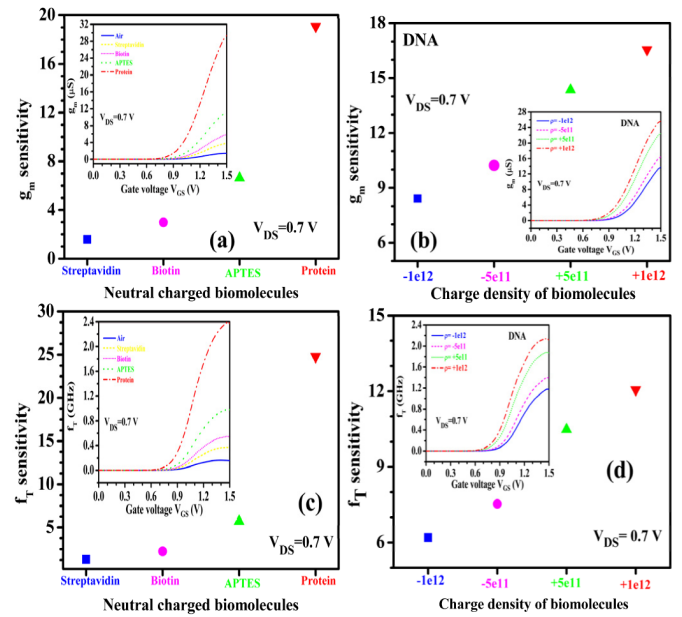


Fig. 10. Transconductance (g_m) sensitivity plot of (a) neutral charge biomolecules (b) charged biomolecules (DNA) and cut-off frequency (f_T) sensitivity plot of (c) neutral charge biomolecules (d) charged biomolecules (DNA).

amplifier is designed by using the proposed device for creating an absolute biosensor for better sensitivity, which can be detected for biasing state. Similarly, Fig. 10(c-d) shows the f_T sensing capability for different biomolecules make it possible to detect and distinguish various dielectric as well as charge density of biomolecules at high frequency.

The requirement of high-speed biosensors is increasing due to its utilization in many electronic circuits. The sensing speed of the biosensor is measured by the transit time (τ) of the device.

Transit time is described as the time needed for the charge carriers (electron or hole) to travel the distance between the source and drain region of the device. Transit time (τ) is reciprocal of cut-off frequency (f_T) and expressed as given below:

$$\tau = \frac{1}{2\pi f_T} \quad (6)$$

Fig. 11(a-d) shows the value of transit time (τ) as a function of applied V_{GS} for four different neutral biomolecules. With an increase in the dielectric constant from $k = 2.1$ to $k = 8$, smaller time taken by the electron to reach from source to drain region, which leads to high speed and the better response of the biosensor. From all four figures, it is seen that at higher V_{GS} , streptavidin and protein show lower and higher variation respectively for transit time.

Device efficiency (g_m/I_d) is the parameter, which is used to measure the ability of the device to convert the drain current (I_d) into g_m . However, to analyze the applicability of device efficiency (g_m/I_d) as a sensing parameter for proposed biosensor in Fig. 12 (a-d), we have plotted the g_m/I_d graph with respect to the applied V_{GS} .

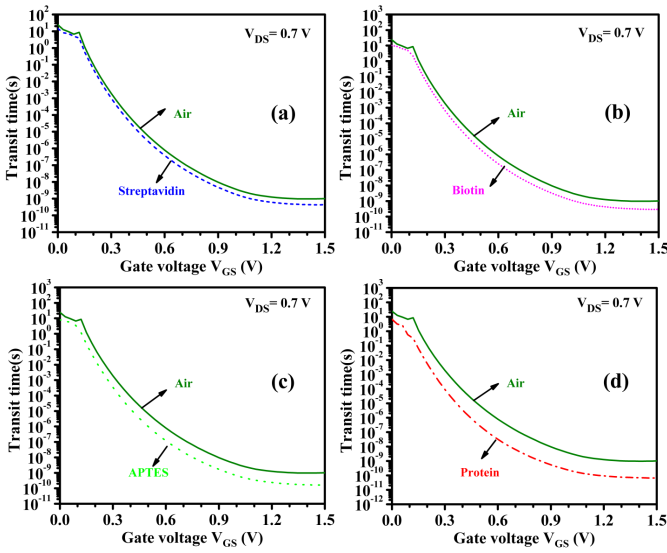


Fig. 11. Variation of transit time (T) with V_{GS} for (a) streptavidin (b) biotin (c) APTES and (d) protein.

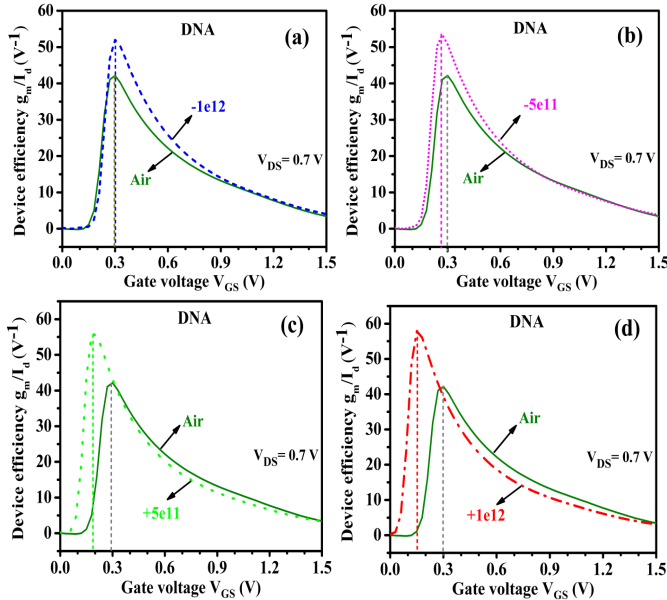


Fig. 12. Variation of device efficiency (g_m/I_d) with V_{GS} for different charge density of DNA (a) $-1e12$ (b) $-5e11$ (c) $+5e11$ and (d) $+1e12$.

The biosensor is turned ON at higher V_{GS} , so lower values of g_m/I_d are obtained. But at lower value of V_{GS} , the device is in OFF-state, results in higher values of g_m/I_d . The peak values of g_m/I_d slightly enhanced as the DNA charge density increases from negative to positive.

However, approximately at the same V_{GS} , peaks of g_m/I_d for air and $(-1e12)$ negative charge density is obtained (Fig. 12 (a)). As the charge density increases, peak of g_m/I_d shifted towards the lower value of V_{GS} .

For example, peak of g_m/I_d is achieved for charge density $-5e11$, $+5e11$ and $+1e12$, at applied V_{GS} of 0.26V , 0.195V and 0.15V respectively (Fig 12 (b-d)). From the observation, it can be signified that g_m/I_d facilitate the detection of various

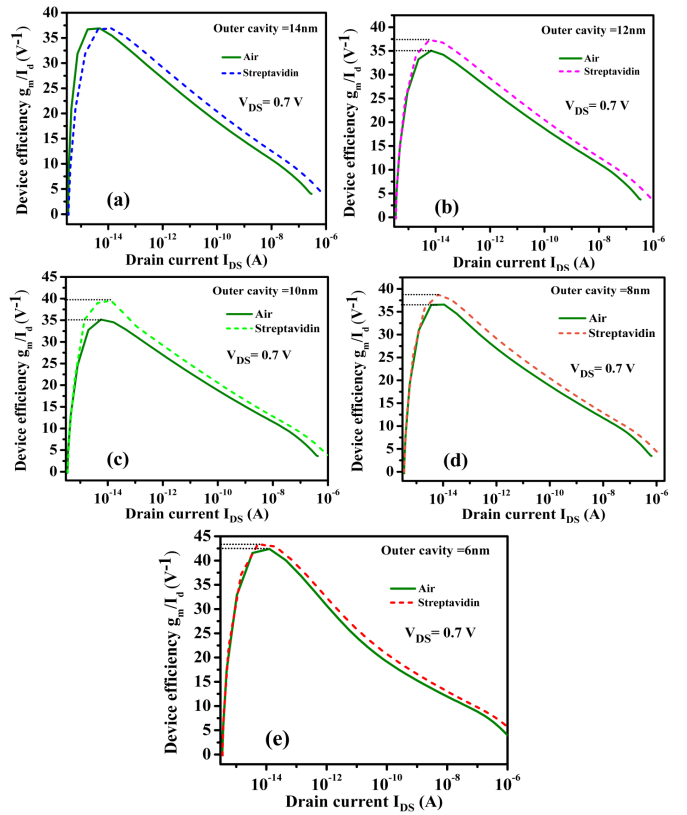


Fig. 13. Variation of device efficiency (g_m/I_d) with respect to I_{DS} for streptavidin for outer cavity lengths of (a) 14nm (b) 12nm (c) 10nm (d) 8nm and (e) 6nm.

charge density of DNA biomolecules within the nanogap cavity.

C. Optimization

Optimization of the outer cavity length is done by using device efficiency (g_m/I_d) as a function of I_{DS} . Fig. 13 (a-e) observes the impact of outer cavity length (14nm to 6nm) on the device efficiency (g_m/I_d) for streptavidin ($k = 2.1$). For the wider cavity length (14nm), the peak value of g_m/I_d for streptavidin is slightly right side shifted for I_{DS} , but the magnitude of g_m/I_d for both air and streptavidin are equal as shown in Fig. 13 (a). This signifies that control of the outer gate for tunneling junction is not much affected. Similarly, from Fig. 13 (b-e) when cavity length reduced from 12nm to 6nm, the peak value of g_m/I_d increases as compared to air, but for cavity length 10nm, peak value of g_m/I_d as well as variation in peak value is higher. This observation indicates that at 10nm cavity length outer gate controllability over the channel region is higher. So, 10nm outer cavity length is considered for better sensing capability of the proposed biosensor.

To show the presence of biomolecules in an individual (inner or outer) and both the cavities at a time, optimization of cavity is performed. Fig. 14(a) shows that I_{DS} sensitivity is lower for streptavidin ($K = 2.1$) and APTES ($K = 3.57$) when biomolecules are present only in the inner cavity. The diagram of I_{DS} sensitivity demonstrates that for every nanogap cavities, sensitivity increases with K . The inner and outer nanogap

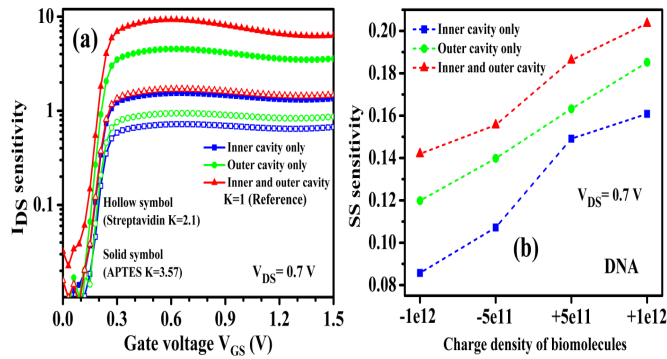


Fig. 14. Sensitivity of (a) drain current for different dielectric constant (K) (b) subthreshold swing for negative and positive charge density.

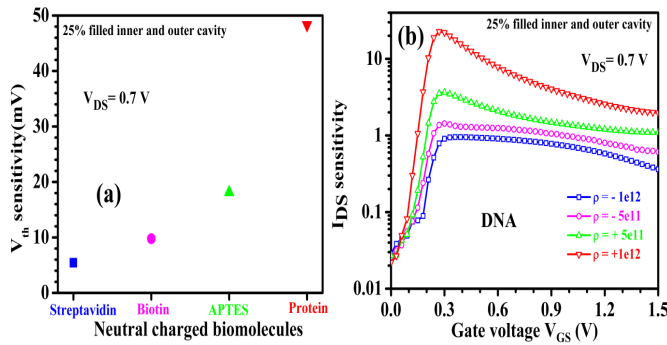


Fig. 15. Sensitivity of (a) threshold voltage for different dielectric constant (K) (b) drain current for negative and positive charge density.

cavity together provides a large area for stabilizing biomolecules but also enhanced the biosensor's sensing capability.

Apart from this, the SS sensitivity has been examined in Fig. 14(b); SS sensitivity increases from higher negative to higher positive charge density of DNA biomolecules. Here inner, and outer cavities together perform better in SS sensitivity than other individuals (inner or outer) nanogap cavities activated alone at the same time. So, inner and outer cavities together at a time provide higher sensitivity for the detection of biomolecules in the proposed nanotube sensor.

Further, the effect of 25% filled biomolecules in inner and outer nanogap cavities are explained in Fig. 15(a) and (b). As both the nanogap cavities are filled with 25% of different biomolecules, as shown in Fig. 15(a), the V_{th} sensitivity increases with increase in the dielectric constant K of the biomolecule. Similarly, I_{DS} sensitivity is shown in Fig. 15(b) when DNA with different charge densities is 25% filled in the inner and outer cavity. Here, we can see an increment in the I_{DS} sensitivity from higher negative to higher positive charge density of DNA biomolecules. Based on this sensing performance, the proposed nanotube biosensor has better sensitivity for biomolecules when inner and outer cavities are partially 25% filled with the biomolecules.

V. CONCLUSION

In this manuscript, a charge plasma-based dual cavity nanotube TFET (DC-NT-TFET) device is analyzed for the detection of neutral and charged biomolecules. This man-

script offers an idea about the internal physics of the proposed biosensor in terms of various DC and RF FOMs. The results indicate that for different biomolecules, RF parameters shows higher sensitivity as compared to DC parameter sensitivity within the nanogap cavity. However, the entire sensitivity factor is increasing the function of dielectric constant and charge density of biomolecules.

REFERENCES

- M. Barbaro, A. Bonfiglio, and L. Raffo, "A charge-modulated FET for detection of biomolecular processes: Conception, modeling, and simulation," *IEEE Trans. Electron Devices*, vol. 53, no. 1, pp. 158–166, Jan. 2006.
- X. Chen *et al.*, "Electrical nanogap devices for biosensing," *Mater. Today*, vol. 13, no. 11, pp. 28–41, Nov. 2010.
- C.-H. Kim, C. Jung, H. G. Park, and Y.-K. Choi, "Novel dielectric-modulated field-effect transistor for label-free DNA detection," *Biochip J.*, vol. 2, no. 2, pp. 127–134, Jun. 2008.
- J.-Y. Kim *et al.*, "An underlap channel-embedded field-effect transistor for biosensor application in watery and dry environment," *IEEE Trans. Nanotechnol.*, vol. 11, no. 2, pp. 390–394, Mar. 2012.
- X. P. A. Gao, G. Zheng, and C. M. Lieber, "Subthreshold regime has the optimal sensitivity for nanowire FET biosensors," *Nano Lett.*, vol. 10, no. 2, pp. 547–552, Feb. 2010.
- N. Kannan and M. J. Kumar, "Dielectric-modulated impact-ionization MOS transistor as a label-free biosensor," *IEEE Electron Device Lett.*, vol. 34, no. 12, pp. 1575–1577, Dec. 2013.
- E. Stern *et al.*, "Label-free immune detection with CMOS-compatible semiconducting nanowires," *Nature*, vol. 445, pp. 519–522, Feb. 2007.
- H. Im, X.-J. Huang, B. Gu, and Y.-K. Choi, "A dielectric-modulated field-effect transistor for biosensing," *Nature Nanotechnol.*, vol. 2, no. 7, pp. 430–434, Jul. 2007.
- V. Passi *et al.*, "High gain and fast detection of warfare agents using back-gated silicon-nanowired MOSFETs," *IEEE Electron Device Lett.*, vol. 32, no. 7, pp. 976–978, Jul. 2011.
- J.-H. Ahn, S.-J. Choi, J.-W. Han, T.-J. Park, S. Y. Lee, and Y.-K. Choi, "Double-gate nanowire field effect transistor for a biosensor," *Nano Lett.*, vol. 10, no. 8, pp. 2934–2938, 2010.
- E. Buitrago *et al.*, "The top-down fabrication of a 3D-integrated, fully CMOS-compatible FET biosensor based on vertically stacked SiNWs and FinFETs," *Sens. Actuators B, Chem.*, vol. 193, pp. 400–412, Mar. 2014.
- A. Zhang and C. M. Lieber, "Nano-bioelectronics," *Chem. Rev.*, vol. 116, no. 1, pp. 215–257, 2016.
- D. Singh, S. Pandey, K. Nigam, D. Sharma, D. S. Yadav, and P. Kondekar, "A charge-plasma-based dielectric-modulated junctionless TFET for biosensor label-free detection," *IEEE Trans. Electron Devices*, vol. 64, no. 1, pp. 271–278, Jan. 2017.
- M. Patil, A. Gedam, and G. P. Mishra, "Performance assessment of a cavity on source charge plasma TFET-based biosensor," *IEEE Sensors J.*, vol. 21, no. 3, pp. 2526–2532, Feb. 2021.
- M. Verma, S. Tirkey, S. Yadav, D. Sharma, and D. S. Yadav, "Performance assessment of a novel vertical dielectrically modulated TFET-based biosensor," *IEEE Trans. Electron Devices*, vol. 64, no. 9, pp. 3841–3848, Sep. 2017.
- Mahalaxmi, B. Acharya, and G. P. Mishra, "Design and analysis of dual-metal-gate double-cavity charge-plasma-TFET as a label free biosensor," *IEEE Sensors J.*, vol. 20, no. 23, pp. 13969–13975, Dec. 2020.
- P. Ajay, R. Narang, M. Saxena, and M. Gupta, "Model of GaSb-InAs p-i-n gate all around biotunnel FET," *IEEE Sensors J.*, vol. 19, no. 7, pp. 2605–2612, Apr. 2019.
- S. Shreya, A. H. Khan, N. Kumar, S. I. Amin, and S. Anand, "Core-shell junctionless nanotube tunnel field effect transistor: Design and sensitivity analysis for biosensing application," *IEEE Sensors J.*, vol. 20, no. 2, pp. 672–679, Jan. 2020.
- A. N. Hanna and M. M. Hussain, "Si/Ge hetero-structure nanotube tunnel field effect transistor," *J. Appl. Phys.*, vol. 117, no. 1, Jan. 2015, Art. no. 014310.
- A. N. Hanna, H. M. Fahad, and M. M. Hussain, "InAs/Si heterojunction nanotube tunnel transistors," *Sci. Rep.*, vol. 5, no. 1, Apr. 2015, Art. no. 9843.

- [21] H. M. Fahad, C. E. Smith, J. P. Rojas, and M. M. Hussain, "Silicon nanotube field effect transistor with core–shell gate stacks for enhanced high-performance operation and area scaling benefits," *Nano Lett.*, vol. 11, no. 10, pp. 4393–4399, Oct. 2011.
- [22] G. Musalgaonkar, S. Sahay, R. S. Saxena, and M. J. Kumar, "Nanotube tunneling FET with a core source for ultrasteep subthreshold swing: A simulation study," *IEEE Trans. Electron Devices*, vol. 66, no. 10, pp. 4425–4432, Oct. 2019.
- [23] G. Musalgaonkar, S. Sahay, R. S. Saxena, and M. J. Kumar, "A line tunneling field-effect transistor based on misaligned core–shell gate architecture in emerging nanotube FETs," *IEEE Trans. Electron Devices*, vol. 66, no. 6, pp. 2809–2816, Jun. 2019.
- [24] B. Ghosh and M. W. Akram, "Junctionless tunnel field effect transistor," *IEEE Electron Device Lett.*, vol. 34, no. 5, pp. 584–586, May 2013.
- [25] S. Busse, V. Scheumann, B. Menges, and S. Mittler, "Sensitivity studies for specific binding reactions using the biotin/streptavidin system by evanescent optical methods," *Biosensors Bioelectron.*, vol. 17, no. 8, pp. 704–710, Aug. 2002.
- [26] Z. Ahangari, "Performance assessment of dual material gate dielectric modulated nanowire junctionless MOSFET for ultrasensitive detection of biomolecules," *RSC Adv.*, vol. 6, no. 92, pp. 89185–89191, 2016.
- [27] E. Makarona *et al.*, "Vertical devices of self-assembled hybrid organic/inorganic monolayers based on tungsten polyoxometalates," *Microelectron. Eng.*, vol. 85, nos. 5–6, pp. 1399–1402, May 2008.
- [28] H. M. Fahad and M. M. Hussain, "High-performance silicon nanotube tunneling FET for ultralow-power logic applications," *IEEE Trans. Electron Devices*, vol. 60, no. 3, pp. 1034–1039, Mar. 2013.
- [29] K. Boucart and A. M. Ionescu, "Double-gate tunnel FET with high-K gate dielectric," *IEEE Trans. Electron Devices*, vol. 54, pp. 1725–1733, Jul. 2007.
- [30] S. Eckhardt, P. S. Brunetto, J. Gagnon, M. Priebe, B. Giese, and K. M. Fromm, "Nanobio silver: Its interactions with peptides and bacteria, and its uses in medicine," *Chem. Rev.*, vol. 113, no. 7, pp. 4708–4754, Jul. 2013.
- [31] Y. Tauran, A. Brioude, A. W. Coleman, M. Rhimi, and B. Kim, "Molecular recognition by gold, silver and copper nanoparticles," *World J. Biol. Chem.*, vol. 4, no. 3, pp. 35–63, 2013.
- [32] M. Ohring, *The Materials Science of Thin Films*. San Diego, CA, USA: Academic, 1991.
- [33] *ATLAS User's Manual Device Simulation Software*, Silvaco Int., Santa Clara, CA, USA, 2015.
- [34] R. J. E. Huetting, B. Rajasekharan, C. Salm, and J. Schmitz, "The charge plasma P–N diode," *IEEE Electron Device Lett.*, vol. 29, no. 12, pp. 1367–1369, Dec. 2008.
- [35] B. Rajasekharan, R. J. E. Huetting, C. Salm, T. van Hemert, R. A. M. Wolters, and J. Schmitz, "Fabrication and characterization of the charge-plasma diode," *IEEE Electron Device Lett.*, vol. 31, no. 6, pp. 528–530, Jun. 2010.
- [36] A. Gedam, B. Acharya, and G. P. Mishra, "Junctionless silicon nanotube TFET for improved DC and radio frequency performance," *Silicon*, vol. 13, no. 1, pp. 167–178, Feb. 2020.
- [37] F. Gossenberger, T. Roman, K. Forster-Tonigold, and A. Groß, "Change of the work function of platinum electrodes induced by halide adsorption," *Beilstein J. Nanotechnol.*, vol. 5, pp. 152–161, Feb. 2014.
- [38] S. Kanungo, S. Chattopadhyay, P. S. Gupta, K. Sinha, and H. Rahaman, "Study and analysis of the effects of SiGe source and pocket-doped channel on sensing performance of dielectrically modulated tunnel FET-based biosensors," *IEEE Trans. Electron Devices*, vol. 63, no. 6, pp. 2589–2596, Jun. 2016.
- [39] Y. Zhu and M. K. Hudait, "Low-power tunnel field effect transistors using mixed as and sb based heterostructures," *Nanotechnol. Rev.*, vol. 2, no. 6, pp. 637–678, Dec. 2013.
- [40] K. Boucart and A. M. Ionescu, "Threshold voltage in tunnel FETs: Physical definition, extraction, scaling and impact on IC design," in *Proc. IEEE 37th Eur. Solid State Device Res. Conf. (ESSDERC)*, Sep. 2007, pp. 299–302.



Anju Gedam (Graduate Student Member, IEEE) received the B.E. degree in electronics and telecommunication engineering from CSVTU Bhilai, India, in 2013, and the M.Tech. degree in micro-nano electronics from the PDPM Indian Institute of Information Technology, Design and Manufacturing, Jabalpur, India, in 2017. She is currently pursuing the Ph.D. degree in electronics and communication engineering with the National Institute of Technology at Raipur, Raipur, India. Her current research interests include tunnel field-effect transistor and its applications, nanoscale device design, and biosensor.



Bibhudendra Acharya received the M.Tech. and Ph.D. degrees in electronics and communication engineering from the National Institute of Technology at Rourkela, Rourkela, India. He is currently serving as the Head of the Central Computer Center and an Assistant Professor with the Department of Electronics and Communication Engineering, National Institute of Technology at Raipur, Raipur, India. He has more than 75 research publications in national/internationals journals and conferences. His research interests include cryptography and network security, microcontroller and embedded systems, signal processing, and mobile communication.



Guru Prasad Mishra (Member, IEEE) received the B.E. degree in electronics engineering from Utkal University, the M.Tech. degree from NIT Rourkela, Rourkela, India, and the Ph.D. degree in electron devices from Jadavpur University, Kolkata, India, in 2012. He is working as an Associate Professor at the National Institute of Technology at Raipur. His current research interests include design, simulation, micro, and nano device.